scientific reports

OPEN

Numerical demonstration of a switchable binary-state metasurface for the spin hall effect of circularly polarized light

Sangmin Shim[1], Kyung-Hyun Yu[1], Minkyung Kim[2]✉ & Dasol Lee[1]✉

The spin Hall effect of light, a transverse and spin-dependent splitting at an optical interface, generally depends on the interface properties. By contrast, the spin Hall effect of circularly polarized light is interface-independent, which aids precise nanoscale displacement control. However, the spin Hall-shifted beam generally exhibits low efficiency near normal incidence, where the shift is large. The static nature of metasurfaces with in-plane anisotropy that have been proposed to address this limitation renders them unsuitable for dynamic or reconfigurable applications. In this study, we numerically demonstrated an electrically tunable metasurface that enabled binary-state switching between spin-Hall-shifted and suppressed reflection efficiencies. The metasurface comprised a grating structure and an indium tin oxide layer, whose permittivity was dynamically modulated via an electrical bias, resulting in changes in the reflection amplitude and phase, and thus, in the spin Hall efficiency. Without an applied voltage, the metasurface exhibited suppressed reflection in the spin-Hall-shifted component. By contrast, the dominance switched to spin Hall-shifted reflection upon voltage application. This approach enables the selective control of the spin-dependent reflection intensity without altering the beam displacement, thereby facilitating reconfigurable spin-optical photonic systems.

Keywords The spin Hall effect of light, Photonic spin hall effect, Switching, Metasurface, Circular polarization

The spin Hall effect of light (SHEL) refers to the transverse displacement of light depending on its polarization components, which occurs upon reflection or refraction at an interface (Fig. 1a)[1–7]. This phenomenon is analogous to the spin Hall effect observed in electrons, because it involves spin-dependent transverse displacement[8]. Although the refraction and reflection of light are generally explained by Snell's law in classical optics, SHEL subtly alters the light trajectory owing to the continuous wave profile in the three-dimensional wave vector space and the transversality of light.

SHEL depends on the polarization state of the incident light. Among various cases, the spin Hall effect of linearly polarized light has been extensively studied. The incident light can be decomposed into left and right-circularly polarized (LCP and RCP) components that experience equal and opposite transverse shifts (Fig. 1b). The magnitude of the shift is determined by the transmission or reflection coefficients, incident angle, and wavelength. Additionally, the spin Hall shift depends on the interface under other polarizations, which is referred to as the interface dependence. One exception is circularly polarized light. In this case, the spin Hall shift depends only on the incident angle and wavelength and not on the transmission or reflection coefficients of the interface. By providing a spin Hall shift that remains constant regardless of the interface, this approach ensures reproducibility and facilitates precise control of beam displacement at the nanoscale across diverse platforms[9]. However, the efficiency, which represents the ratio between the incident and spin Hall-shifted light, continues to be influenced by the optical properties of the interface[10,11].

Despite this interesting aspect of circularly polarized incident light, achieving a high-efficiency interface-independent SHEL remains challenging owing to the intrinsic optical properties of conventional interfaces. In particular, when the phase difference between *s*-polarized and *p*-polarized components approaches π, as is typical in isotropic–isotropic interfaces, the reflected circularly polarized light undergoes handedness reversal[11].

[1]Department of Biomedical Engineering, Yonsei University, Wonju 26493, Republic of Korea. [2]School of Mechanical and Robotics Engineering, Gwangju Institute of Science and Technology (GIST), Gwangju 61005, Republic of Korea. ✉email: m.kim@gist.ac.kr; dasol@yonsei.ac.kr

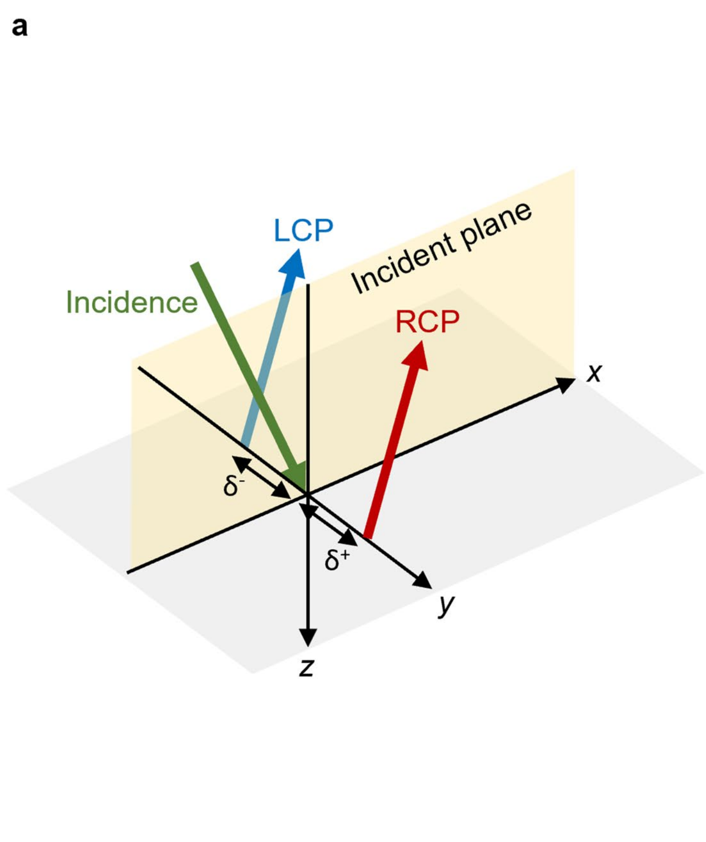

Fig. 1. Schematic of the SHEL. (**a**) SHEL. (**b**) Beam profile at the interface with linearly polarized light incidence. (**c**,**d**) Beam profile at the ITO-based metasurface with/without electrical voltage under left-circularly polarized light incidence.

Consequently, the handedness-preserved component, which is responsible for the spin Hall shift, weakens considerably and leads to poor SHEL efficiency. This limitation renders the precise control of SHEL-based optical responses challenging and hinders their practical applications. To overcome this limitation, a previous study employed a metasurface engineered to minimize the phase difference between *s* and *p* polarizations[10]. However, the optical properties of the metasurface remained unchanged, regardless of the external stimuli. This static nature rendered the metasurfaces unsuitable for reconfigurable or adaptive systems. Integrating materials with externally controllable optical properties into metasurfaces solves this problem[12–27].

In this study, we numerically demonstrated the interface-independent spin Hall shifts with voltage-controlled efficiency switching by using a voltage-switchable metasurface based on indium tin oxide (ITO), a material whose complex permittivity can be actively modulated by external electrical stimuli. The application or removal of the voltage altered the reflection coefficients and phase difference between the *s* and *p* polarizations, enabling discrete control over the SHEL response[24–26]. The proposed metasurface consisted of a grating and multilayer structure incorporated with an ITO layer. This structure supported interface-independent spin Hall shifts under circularly polarized incidence; however, its efficiency switched between two distinct states depending on the applied voltage. Under an applied voltage, the spin Hall shifts, and the handedness-preserved component reflects dominantly. By contrast, the handedness-reversed component is effectively suppressed in intensity (Fig. 1c). The situation was reversed in the absence of an applied voltage: the handedness-preserved component remains weak, whereas the reflected beam is dominated by the handedness-reversed component (Fig. 1d). Although the reflected intensities varied, the magnitude of the spin Hall shift remained interface-independent, which was consistent with the fundamental properties of circularly polarized light. This allows selective control over spin-dependent reflection and facilitates reconfigurable and compact photonic systems with potential applications in optical sensing and polarization-selective modulation[31,32].

Methods

We revisit the derivation of the spin Hall shift and efficiency equation of the reflected beam under arbitrarily polarized incidence. We focused on the interfaces where polarization conversion did not occur ($r_{sp} = r_{ps} = 0$), which holds for our metasurface. An incident Gaussian beam is expressed as the product of the Jones vector representing the polarization state and the scalar function representing the Gaussian beam shape[10]:

$$\psi_i = \begin{pmatrix} \psi_H \\ \psi_V \end{pmatrix} \exp\left(-k_0 \frac{x_i^2 + y_i^2}{z_R + iz_i} + ik_0 z_i\right), \tag{1}$$

where ψ_H and ψ_V represent the complex elements of the Jones vector for horizontal and vertical components, respectively; k_0 is the wave vector ($k_0 = 2\pi/\lambda$); $z_R = k_0 w_0^2/2$ is the Rayleigh length; w_0 is the beam waist; and (x_i, y_i, z_i) are the coordinates of the incident beam. A beam reflected at an interface with reflection coefficients r_p and r_s is given by[33]

$$\psi_r = \begin{pmatrix} \psi_H r_p \left(1 - i\frac{x_r}{z_R + iz_r}\frac{\partial \ln r_p}{\partial \theta_i}\right) + i\psi_V \frac{y_r}{z_R + iz_r}(r_p + r_s)\cot\theta_i \\ \psi_V r_s \left(1 - i\frac{x_r}{z_R + iz_r}\frac{\partial \ln r_s}{\partial \theta_i}\right) - i\psi_H \frac{y_r}{z_R + iz_r}(r_p + r_s)\cot\theta_i \end{pmatrix} \exp\left(-k_0 \frac{x_r^2 + y_r^2}{z_R + iz_r} + ik_0 z_r\right), \tag{2}$$

where (x_r, y_r, z_r) are the coordinates of the reflected beam; θ_i is the incident angle. Reflection coefficients may be derived analytically via the Fresnel equations or computed numerically using simulations with periodic boundary conditions. Because the polarization in Eq. (2) is represented in the linear basis, we multiply ψ_r by $e^{\pm} = (1, \pm i)^T/\sqrt{2}$ to change it to a circular basis as follows:

$$\psi_r^{\pm} = e^{\mp} \cdot \psi_r. \tag{3}$$

The superscript ± indicates the circular polarization direction of the reflected light (+ denotes LCP and – denotes RCP). Inserting $x_r = 0$ in Eq. (2) and applying the first-order Taylor expansion, $1 + \alpha \approx \exp(\alpha)$, the reflected light is expressed in the circular basis as follows:

$$\psi_r^{\pm}(x_r = 0) = \frac{1}{\sqrt{2}}(\psi_H r_p \mp i\psi_V r_s)\exp\left[-\frac{k_0}{2(z_R + iz_r)} \times \left(y_r \pm \frac{\psi_H \mp i\psi_V}{\psi_H r_p \mp i\psi_V r_s}\frac{r_p + r_s}{k_0}\cot\theta_i\right)^2\right]. \tag{4}$$

In Eq. (4), the first term on the right-hand side represents the complex constant governed by the incident polarization and reflection coefficients. By contrast, the second term represents the shape of the reflected Gaussian beam shifted along the y-axis. Using Eq. (4), the spin Hall shift equation under an arbitrary incident polarization can be represented as

$$\delta^{\pm} = \mp \mathrm{Re}\left(\frac{\psi_H \mp i\psi_V}{\psi_H r_p \mp i\psi_V r_s}\frac{r_p + r_s}{k_0}\cot\theta_i\right). \tag{5}$$

This equation indicates the dependence of the spin Hall shift on the reflection coefficients, which only vanishes when the phase difference of the horizontal and vertical components of the incidence is ± π/2. Thus, only under circular polarization ($\psi_H^{\pm} = 1/\sqrt{2}$, $\psi_V^{\pm} = \pm i/\sqrt{2}$), the spin Hall shift is interface-independent, exhibiting $\delta^{\pm} = \mp 2\cot\theta_i/k_0$ for handedness-preserved light and zero for handedness-reserved. Therefore, under circular polarization, SHEL occurs only for handedness-preserved light, and the corresponding spin Hall shift is solely determined by the incident angle and wavelength[34]. This behavior contrasts with that of the SHEL under linearly or elliptically polarized beams, in which the spin Hall shift is determined by the reflection coefficients of the interface.

Meanwhile, the efficiency ε of the spin Hall shifted beam from the interface contains the reflection coefficients as

$$\varepsilon^{\pm} = |\psi_H r_p \mp i\psi_V r_s|^2/2, \tag{6}$$

and is interface-dependent, unlike the spin Hall shift. This is because Eq. (5) only considers λ and θ_i, whereas ε involves the reflection coefficients of the interface[11]. Equations (5) and (6) are applicable only when $k_0^2 w_0^2 \gg \cot^2\theta_i$ and may provide incorrect results at sufficiently small θ_i, at which higher-order terms in the Taylor expansion become non-negligible.

Results and discussions

We designed a multilayered metasurface composed of aluminum (Al) mirror, hafnium dioxide (HfO_2), aluminum oxide (Al_2O_2), and ITO layers, and gold (Au) grating to enable optical property modulation through applied voltage. By utilizing this structure, we aimed to achieve binary-state switchability through electrical modulation. The grating structure introduced in-plane anisotropy, which enhances the SHEL at small incident angles[35]. ITO's characteristics—such as switching speeds in the MHz to low-GHz range and femtojoule-level energy consumption per bit—have enabled its use in a wide range of practical applications[36,37]. Our simulation was based on experimentally validated parameters reported by Park et al.[14], in which the refractive index variations of ITO under different applied voltages were characterized. Based on these empirical results, our simulation is expected to exhibit behavior that is closely aligned with practical implementations. The reflection coefficients of the ITO-based metasurface were numerically obtained based on a two-step simulation framework reported in a previous study[14]. Specifically, the voltage-dependent carrier distribution in the ITO layer, discretized into 0.025 nm-thick sublayers, was computed using Synopsys Technology computer-aided design software under the assumption of one-dimensional planar symmetry. A background carrier density of $4.0 \times 10^{20}\ \mathrm{cm}^{-3}$. Using the Drude model[38], the corresponding voltage-dependent complex permittivity profiles for each ITO sublayer were derived and subsequently incorporated into finite element method implemented in COMSOL Multiphysics to calculate the reflection coefficients of the metasurface. These simulations were conducted under a time-harmonic assumption using a wave function of the form $\exp\left[\mathrm{i}\left(\omega\,\mathrm{t}-\vec{\mathrm{k}}\bullet\vec{\mathrm{x}}\right)\right]$, where ω is the angular frequency, t is time, and $\vec{\mathrm{k}}$ and $\vec{\mathrm{x}}$ are the wavevector and spatial coordinates, respectively. It is noted that surface plasmon resonances at the Au/ITO interface induce strong local field enhancements near the surface plasmon resonance wavelength (~ 1.30 μm), resulting in pronounced dips in reflection amplitude and sudden phase shifts that directly affect the SHEL efficiency.

The metasurface structure consisted of a 70-nm-thick Al mirror at the bottom, which served as the bottom electrode to which an electrical bias (V_b) was applied; a bottom insulator layer, a 5-nm-thick ITO layer, an upper insulator layer, and an Au grating with a thickness of 50 nm, width of 175 nm, and grating period of 370 nm, which served as the top electrode under electrical bias (V_t) (Fig. 2a). The HfO_2 and Al_2O_2 layers, consisting of 7 nm of HfO_2 and 1 nm of Al_2O_2, functioned as the upper and bottom insulators surrounding the ITO layer. By adjusting the applied voltages at the top and bottom electrodes, the charge carrier concentration in the ITO layer was modulated, leading to charge accumulation and depletion at the interfaces with the surrounding insulators, which in turn directly altered the permittivity of the ITO and thereby modulated both the reflection coefficient of the metasurface. Switchable modulation of the metasurface was implemented under two voltage conditions: applied state (V_t = 1.75 V, V_b = 4.7 V) and grounded state (V_t = V_b = 0 V).

Based on prior research[14], distinct reflection coefficients for each polarization were obtained depending on the applied voltage (Fig. 2b,c). This grating-based metasurface was designed to induce the diffraction of *p*-polarized light. When voltage is applied, the grating structure alters the reflection coefficients of *p*-polarized light, mostly the phase, by redistributing energy through diffraction. By contrast, *s*-polarized light interacts less with the grating structure; thus, its reflection coefficient remains unchanged even when a voltage is applied. This design allows the selective modulation of r_p, without affecting r_s, by applying a voltage.

We numerically calculated the spin Hall shift and its efficiency with and without voltage, under an incident LCP ($\psi_H = 1/\sqrt{2}$, $\psi_V = i/\sqrt{2}$). The following beam parameters were used: wavelength $\lambda = 1.3\,\mu m$, beam waist $w_0 = 100\lambda$, and propagation distance $z_r = 10\,\lambda$. Equation (5) is valid for $\theta_i > 1^\circ$, in which the spin Hall shift is considerably smaller than the beam waist. For $\theta_i < 1^\circ$, the spin Hall shift was calculated using the average *y* position. The efficiencies ϵ_P and ϵ_R were calculated using Eq. (6) under the condition $\theta_i > 1^\circ$

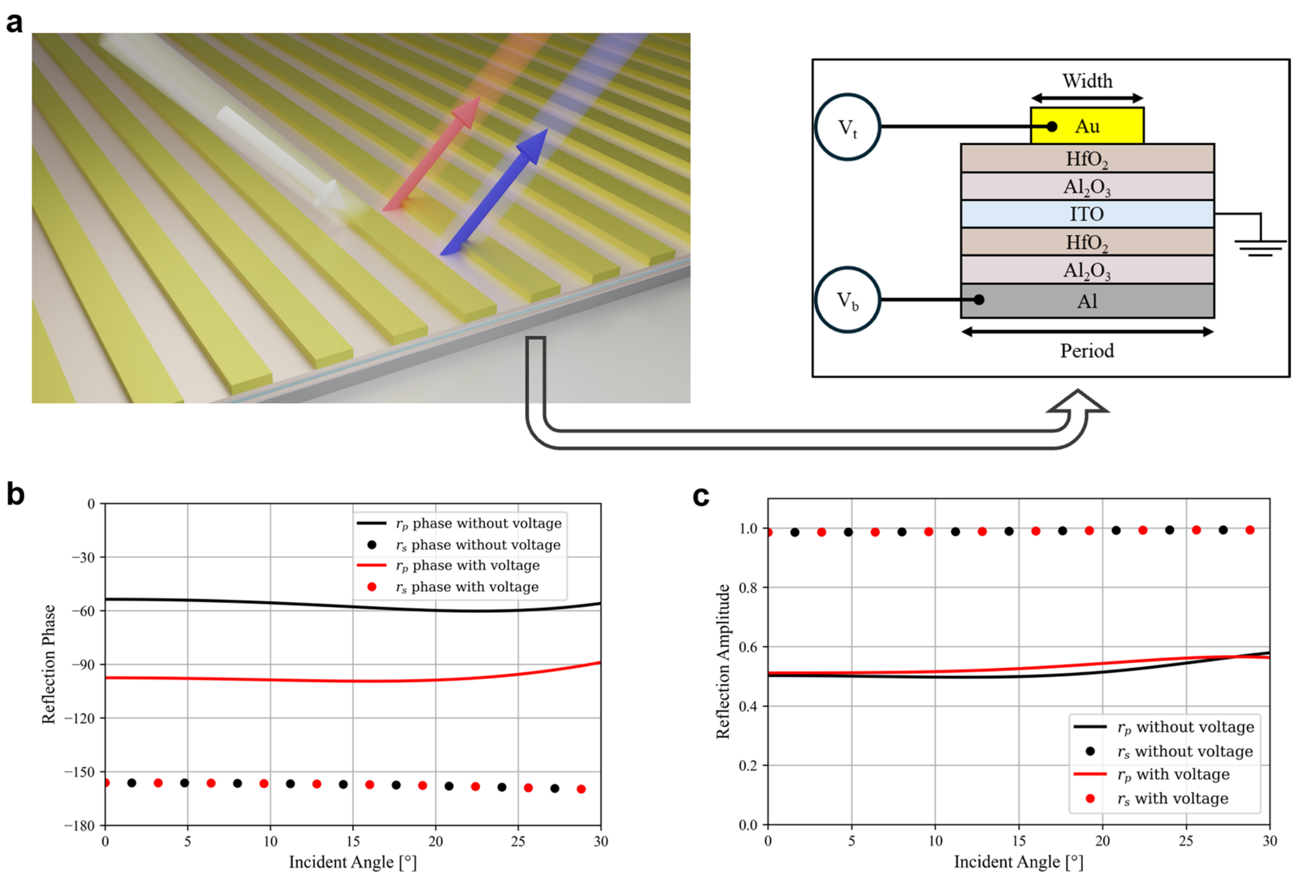

Fig. 2. Schematic of the ITO-based metasurface and its optical properties with and without the electrical voltage. (**a**) Illustration of SHEL at the metasurface (left) and side view of the metasurface, consisting of Au grating, top insulator (HfO_2, Al_2O_2), ITO, bottom insulator (HfO_2, Al_2O_2), and Al layers. (**b**) Reflection phase and (**c**) amplitude of metasurface with and without the electrical voltage.

. For $\theta_i < 1°$, the efficiency was determined by the ratio of intensities of the spin Hall-shifted light to that of the incident light.

We examined the spin Hall shift and efficiency when a voltage was applied to the metasurface. Additionally, the spin Hall shift for RCP (δ^- / λ) was calculated under the same conditions, and no change was observed at any incident angles (red solid line and red markers in Fig. 3a). In both cases, with and without the applied voltage, the spin Hall shift exhibited the same displacement for the handedness-preserved component, whereas no spin Hall shift occurred for the handedness-reversed case. The spin Hall shift was determined only by the incident angle and wavelength, rather than the reflection coefficients or the voltage. This behavior is consistent with the interfacial independence of the spin Hall shift under circularly polarized light. Accordingly, we focused on a small angular range where the spin Hall shift remains sufficiently large to be clearly observed and practically significant.

By contrast, the efficiency was governed by the reflection coefficients of the metasurface, which varied depending on whether voltage was applied. Without the applied voltage, the handedness-reversed efficiency, ϵ_{R} (red solid line in Fig. 3b), was higher than the handedness-preserved efficiency, ϵ_{P} (black solid), across all incident angles. Notably, despite the absence of voltage, ϵ_{P} was nonzero because of the in-plane anisotropy originating from the grating structure. Although ϵ_{P} was negligible for a planar interface or an interface with in-plane isotropy, the grating structure induced a nonzero ϵ_{P}, whose magnitude is relatively small. Conversely, for the metasurface with an applied voltage, ϵ_{P} (black solid line in Fig. 3c) was higher than ϵ_{R} (red solid line in Fig. 3c) for all incident angles. This behavior is primarily attributed to the applied voltage, which reduces the phase difference between two reflection coefficients and significantly enhances ϵ_{P}. These differences arose from the variation in the reflection coefficients with and without applied voltage. Although r_{s} barely changed, r_{p} was typically smaller without an applied voltage than with an applied voltage. This variation directly affected the efficiency, increasing the handedness-reversal efficiency without an applied voltage and the handedness-preserved efficiency with an applied voltage.

Furthermore, we calculated the cross-sectional intensity profiles of the light reflected from the metasurface with and without the applied voltage when the LCP beam was incident at an angle of 0.6°. In the absence of the applied voltage, the RCP beam, which corresponded to the handedness-reversed component, was reflected at a higher intensity (36% of the incident beam) than the LCP beam (25%), which confirmed that ϵ_R dominated over ϵ_P in efficiency. Moreover, the spin Hall shift occurred only in the handedness-preserved beam. Although no observable spin Hall shift was detected for the RCP beam, the LCP beam exhibited a spin Hall shift of 34.84 µm (Fig. 4a).

By contrast, the application of a voltage to the metasurface significantly altered the optical properties, leading to an inversion of the efficiency between ϵ_P and ϵ_R. The reflection of the RCP beam was reduced to 17% of the incident intensity, whereas the LCP reflection was enhanced by up to 43% (Fig. 4b). Despite this significant variation in intensity, the spin Hall shift remained the same with and without the applied voltage. These results were also confirmed by the two-dimensional intensity profiles (Fig. 5a–f).

A circularly polarized beam incident on the metasurface induces SHEL with transverse displacement for the handedness-preserved component. As θ_i increased further, the spin Hall shift decreased, hindering the identification of LCP and RCP. Conversely, the spin Hall shift increased up to half of the beam waist[39] by reducing θ_i. The dependence of the spin Hall shift on the incident angle and wavelength allowed control over the shift by tuning the incident angle. Meanwhile, the efficiency remained voltage-dependent, indicating that the intensity of the reflected components could be independently controlled through the applied voltage, allowing precise control over the efficiency without altering the spin Hall shift.

Conclusion

In summary, we numerically demonstrated an electrically switchable spin Hall effect of circularly polarized light using an ITO-based metasurface, where the spin Hall shift remained interface-independent, whereas the efficiency was voltage-dependent. ITO has been widely reported to exhibit fast and stable switching characteristics, and numerous studies have explored its potential for real-time, low-power, and high-speed optical applications. Motivated by these properties, we utilized a grating-integrated metasurface with an ITO layer and achieved

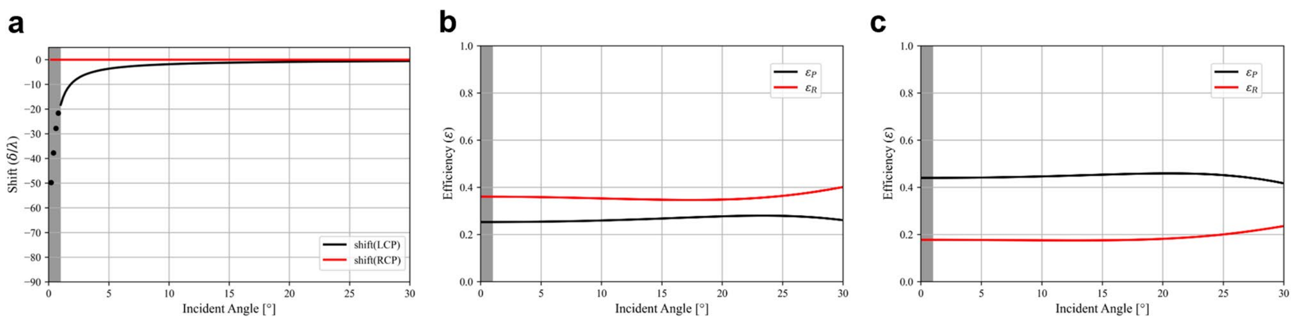

Fig. 3. Spin Hall shift and efficiency under the LCP incidence with and without electric voltage. (**a**) Spin Hall shift of the LCP (black) and RCP (red). Efficiency of the LCP (black) and RCP (red) (**b**) without and (**c**) with electrical voltage.

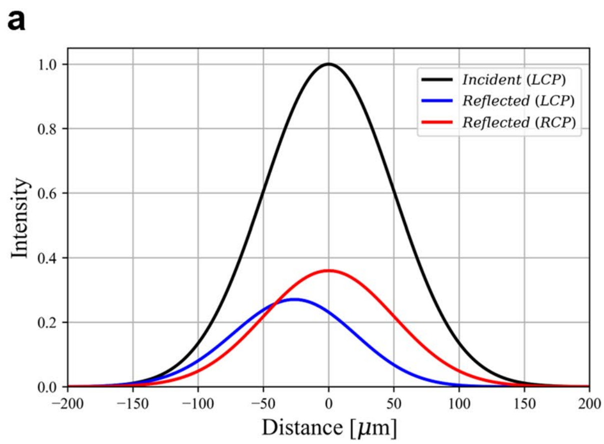

Fig. 4. Intensity profiles of the incident and reflected beams at $\theta_i = 0.6°$. Cross-sectional intensity profiles (**a**) without and (**b**) with voltage.

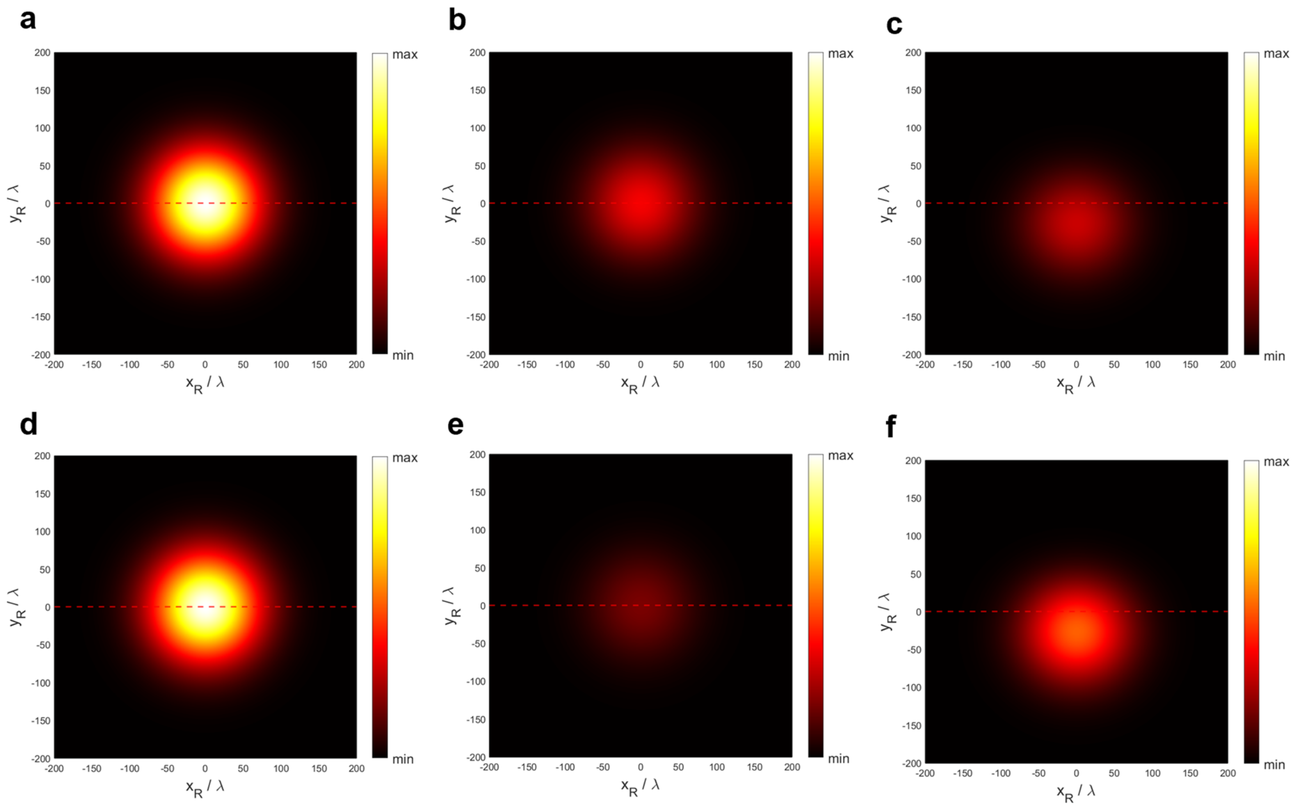

Fig. 5. Two-dimensional intensity profile of the incident and reflected LCP and RCP beams at $\theta_i = 0.6°$. (**a**,**d**) Incident beam profiles with/without voltage. (**b**,**c**) Reflected RCP and LCP beam profiles without voltage. (**e**,**f**) Reflected RCP and LCP beam profiles with voltage. The central dashed line denotes the midpoint along the *y*-axis of the incident beam.

binary-state switchability over the intensity of handedness-preserved and handedness-reversed components without affecting the spin Hall shift. The incident angle served as a primary tuning factor for the spin Hall shift. By contrast, voltage application allowed the independent control of efficiency, leading to inversion in the handedness-dependent reflection behavior. The metasurface enabled switching between handedness-preserved and handedness-reversed efficiencies when a voltage was applied to the top and bottom insulators. The proposed design provides a promising platform for further investigations of switchable SHEL response. Such advancements could enable the development of applications for sensing, spin-based optical communication.

Data availability
All datasets used or analyzed during this research are available from the corresponding author on request.

Received: 13 May 2025; Accepted: 16 July 2025
Published online: 21 July 2025

References
1. Bliokh, K. Y. & Aiello, A. Goos-Hänchen and Imbert-Fedorov beam shifts: an overview. *J. Opt.* **15**, 014001 (2013).
2. Imbert, C. Calculation and experimental proof of the transverse shift induced by total internal reflection of a circularly polarized light beam. *Phys. Rev. D*. **5**, 787–796 (1972).
3. Töppel, F., Ornigotti, M. & Aiello, A. Goos-Hänchen and Imbert-Fedorov shifts from a quantum-mechanical perspective. *New. J. Phys.* **15**, 113059 (2013).
4. Hosten, O. & Kwiat, P. Observation of the spin hall effect of light via weak measurements. *Science*. **319**, 787–790 (2008).
5. Bliokh, K. Y., Rodríguez-Fortuño, F. J., Nori, F. & Zayats, A. V. Spin-orbit interactions of light. *Nat. Photon*. **9**, 796–808 (2015).
6. Onoda, M., Murakami, S. & Nagaosa, N. Hall effect of light. *Phys. Rev. Lett.* **93**, 083901 (2004).
7. Fedorov, F. I. To the theory of total reflection. *J. Opt.* **15**, 014002 (2013).
8. Ling, X. et al. Recent advances in the spin hall effect of light. *Rep. Prog. Phys.* **80**, 066401 (2017).
9. Kim, Y., Li, X., Tang, P., Li, G. & Rho, J. Spin-dependent phenomena of meta-optics. *ACS Photon*. **12**, 16–33 (2025).
10. Kim, M. & Lee, D. Strengthened spin hall effect of circularly polarized light enabled by a single-layered dielectric metasurface. *Mater*. **16**, 283 (2022).
11. Kim, M., Lee, D., Kim, Y. & Rho, J. Generalized analytic formula for spin hall effect of light: shift enhancement and interface independence. *Nanophoton*. **11**, 2803–2809 (2022).
12. Shirmanesh, G. K., Sokhoyan, R., Wu, P. C. & Atwater, H. A. Electro-optically tunable multifunctional metasurfaces. *ACS Nano*. **14**, 6912–6920 (2020).
13. Chae, H. U., Shrewsbury, B., Ahsan, R., Povinelli, M. L. & Kapadia, R. GaAs mid-IR electrically tunable metasurfaces. *Nano Lett.* **24**, 2581–2588 (2024).
14. Park, J. et al. All-solid-state spatial light modulator with independent phase and amplitude control for three-dimensional lidar applications. *Nat. Nanotechnol*. **16**, 69–76 (2021).
15. Karst, J. et al. Electrically switchable metallic polymer nanoantennas. *Science*. **374**, 612–616 (2021).
16. Ko, B. et al. Tunable metasurfaces via the humidity responsive swelling of single-step imprinted Polyvinyl alcohol nanostructures. *Nat. Commun.* **13**, 6256 (2022).
17. Li, M., Chen, W., Liu, P., Xu, F. & Chen, Y. Analysis of mechanically tunable metasurfaces for identifying multiple strains. *Opt. Commun*. **554**, 130201 (2024).
18. Ee, H. S. & Agarwal, R. Tunable metasurface and flat optical zoom lens on a stretchable substrate. *Nano Lett.* **16**, 2818–2823 (2016).
19. Effah, E., Nettey-Oppong, E. E., Ali, A., Byun, K. M. & Choi, S. H. Tunable metasurfaces based on mechanically deformable polymeric substrates. *Photon*. **10**, 119 (2023).
20. Fan, F. et al. Magnetically induced Terahertz birefringence and chirality manipulation in transverse-magnetized metasurface. *Adv. Opt. Mater.* **9**, 2101097 (2021).
21. Armelles, G. et al. Magnetic modulation of far- and near-field IR properties in rod-slit complementary spintronic metasurfaces. *Opt. Exp.* **28**, 32584–32600 (2020).
22. Sharma, G., Lakhtakia, A., Bhattacharyya, S. & Jain, P. K. Magnetically tunable metasurface comprising InAs and InSb pixels for absorbing Terahertz radiation. *Appl. Opt.* **59**, 9673–9680 (2020).
23. Lu, Y., Wang, C., Zhao, S. & Wen, Y. Magnetically tunable graphene-based terahertz metasurface. *Front. Phys.* **8** (2021).
24. Han, C. et al. Allangle unidirectional flatband acoustic metasurfaces. *Nat. Commun.* **16**, 634 (2025).
25. Tian, J. et al. Reconfigurable generation and spin manipulation of structured beams based on cascaded liquid crystal Pancharatnam–Berry phase elements. *Laser Photon. Rev.* **19**, 2401378 (2025).
26. Guo, Z. et al. Polarization-selective unidirectional and bidirectional diffractive neural networks for information security and sharing. *Nat. Commun.* **16**, 4492 (2025).
27. Tan, Z. Y., Fan, F. & Chang, S. J. Active broadband manipulation of Terahertz photonic spin based on gyrotropic Pancharatnam–Berry metasurface. *IEEE J. Sel. Top. Quantum Electron*. **26**, 1–8 (2020).
28. Forouzmand, A., Salary, M. M., Inampudi, S. & Mosallaei, H. A tunable multigate indium-tin-oxide-assisted all-dielectric metasurface. *Adv. Opt. Mater.* **6**, 1701275 (2018).
29. Ma, R., Mao, Y., Li, P., Li, D. & Wen, D. ITO-based electrically tunable metasurface for active control of light transmission. *Nanomater*. **14**, 1606 (2024).
30. Forouzmand, A. et al. Tunable all-dielectric metasurface for phase modulation of the reflected and transmitted light via permittivity tuning of indium Tin oxide. *Nanophoton*. **8**, 415–427 (2019).
31. Zeng, K. et al. Rotational photonic spin hall effect sensor for liquid chemicals classification via EfficientNetV2. *ACS Photonics*. **12**, 485–494 (2024).
32. Ke, Y. et al. Rotational photonic spin hall effect. *Nanophotonics* **12**, 4361–4373 (2023).
33. Aiello, A. & Woerdman, J. P. Role of beam propagation in Goos-Hänchen and Imbert-Fedorov shifts. *Opt. Lett.* **33**, 1437–1439 (2008).
34. Ling, X. et al. Revisiting the anomalous spinhall effect of light near the Brewster angle. *Phys. Rev. A*. **103**, 033515 (2021).
35. Kim, M. et al. Observation of enhanced optical spin hall effect in a vertical hyperbolic metamaterial. *ACS Photon*. **6**, 2530–2536 (2019).
36. Kireev, D. et al. Metaplastic and energy-efficient biocompatible graphene artificial synaptic transistors for enhanced accuracy neuromorphic computing. *Nat. Commun.* **13**, 4386 (2022).
37. Li, E., Zhou, B., Bo, Y. & Wang, A. X. Highspeed femtojoule per bit Siliconconductive oxide nanocavity modulator. *J. Lightwave Technol.* **39**, 178–185 (2021).
38. Saleh, B. E. A. & Teich, M. C. *Fundamentals of Photonics* 2nd edn (Wiley-Interscience, 2007).
39. Miao, C. et al. Limitations of the transmitted photonic spin hall effect through layered structure. *Sci. Rep.* **11**, 21083 (2021).

Acknowledgements
D.L. acknowledges the National Research Foundation (NRF) grants (RS-2025-00556856) funded by the Ministry of Science and ICT (MSIT) of the Korean government. M.K. acknowledges the NRF grants (NRF-2022R1C1C2004662) funded by the MSIT of the Korean government.

Author contributions
S.S.: Writing—review and editing, writing—original draft, visualization, methodology, validation, data curation.

K.-H.Y.: Writing—review and editing, visualization, investigation. M.K.: Writing—review and editing, methodology, formal analysis, resource, conceptualization. D.L.: Writing—review and editing, investigation, formal analysis, conceptualization, validation, funding acquisition.

Declarations

Competing interests
The authors declare no competing interests.

Additional information
Correspondence and requests for materials should be addressed to M.K. or D.L.